iScience

Article

Screen printing of ionic diode arrays for large-area uniform moist-electric generators

Graphical abstract

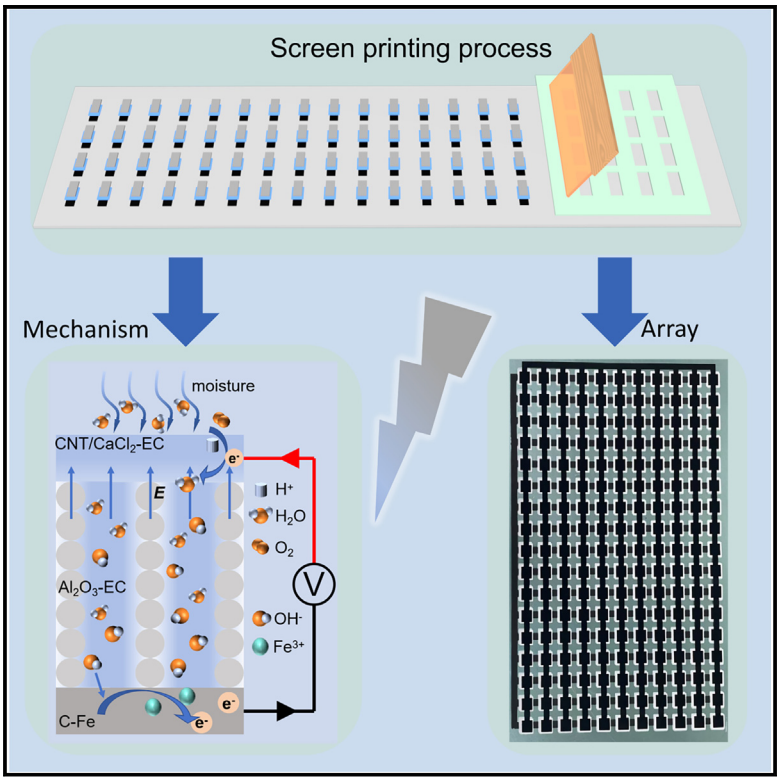

Highlights

- The moisture-based power generation array can be manufactured using screen printing
- The device has a sandwiched ion diode structure facilitating the fast movement of ions
- Sandwich structure shows large PN junction area and good charge collection ability
- After series-parallel integration, the array device can output 126 V and 5.47 mA

Authors

Jie Zhou, Xiang Zhang, Yuming Yao, Tingting Yang

Correspondence

2019111390@my.swjtu.edu.cn (X.Z.), yangtingting@swjtu.edu.cn (T.Y.)

In brief

Energy resources; Power engineering; Energy sustainability; Energy Systems

Zhou et al., 2025, iScience 28, 112026
March 21, 2025
https://doi.org/10.1016/j.isci.2025.112026

CellPress

iScience

CellPress
OPEN ACCESS

Article

Screen printing of ionic diode arrays for large-area uniform moist-electric generators

Jie Zhou,[1,2] Xiang Zhang,[3,*] Yuming Yao,[3] and Tingting Yang[3,4,5,*]
[1]School of Electronic Information and Electrical Engineering, Chengdu University, Chengdu 610100, China
[2]School of Materials Science and Engineering, Tsinghua University, Beijing 100084, China
[3]Tribology Research Institute, School of Mechanical Engineering, Southwest Jiaotong University, Chengdu 610031, P.R. China
[4]Institute of Smart City and Intelligent Transportation, Southwest Jiaotong University, Chengdu 610031, Sichuan, P.R. China
[5]Lead contact
*Correspondence: 2019111390@my.swjtu.edu.cn (X.Z.), yangtingting@swjtu.edu.cn (T.Y.)
https://doi.org/10.1016/j.isci.2025.112026

SUMMARY

Developing moist-electric array device using screen printing technology that meets mass customization, high power output, and wearable capabilities is very attractive for sustainable mobile power. However, the design of sandwich stacked moist-electric array devices and their screen printing patterning manufacturing process are still challenging. Here, we developed a large-scale fine construction strategy for ion diode nano-channels compatible with screen printing process. A single moist-electric device can generate an open circuit voltage of 0.7 V and a short circuit current density of 56.69 μA/cm^2. After large-area integrated manufacturing, the array can generate an open circuit voltage of 126 V and a short circuit current of 5.47 mA. In addition, compared with the spraying process, the performance deviation between different array units is greatly reduced using the screen printing process, which is the key to ensuring the application of moist-electric technology from a single prototype device to a functional integrated device.

INTRODUCTION

Harnessing the energy contained in ambient water to solve energy problems has recently attracted great interest.[1–8] Limited by the weak interaction between moisture and nano-functional materials, the power of moisture-based power generation devices is usually in the μW range.[9–19] Previously reported nano-functional materials for moisture-based power generation devices include bio-nanofibers,[9] polymer electrolyte films,[10,13,14] graphene oxide,[11] wood,[12] and electrospun cellulose acetate nanofiber membranes.[15] In order to further significantly increase the output power and promote the application of functional integrated devices, the researchers used a variety of patterning manufacturing techniques to achieve series and parallel connection of moist-electric devices.[20–26] Compared with other conventional printing manufacturing technologies (inkjet printing, spraying, and blade coating), the thickness of the screen printing ink layer can generally reach about 30 μm, which is far greater than other printing methods and is more suitable for the effective construction of moisture-based power generation layers (the optimal thickness of moisture-based power generation layers is usually tens to hundreds of μm).[26] Moreover, screen printing can be used for large-area printing at the meter level, and its large-area printing uniformity is far superior to other printing methods. For example, Qu et al. manufactured arrayed moist-electric devices based on polyelectrolytes through screen printing.[23] A single device can provide an open circuit voltage of 1.1 V and a power density of 2.6 μW/cm^2. After arrayed integrated manufacturing, 200 units provide an open circuit voltage of 200 V in series and a short circuit current of 1.3 mA in parallel. However, due to the hygroscopic expansion and even dissolution of polyelectrolytes, this screen printing process is only applicable to planar device structures. Compared with planar device structures, sandwich stacking structures have larger PN junction areas and larger electrode charge collection areas, which are more conducive to the efficient separation of opposite charge carriers under moisture stimulation[27–30] and the rapid conversion of charges at the electrodes. Therefore, combining screen printing technology with sandwich stacking structures to manufacture moist-electric devices is expected to further increase the power generation, but it remains to be explored. The challenges are as follows. (1) The ink design needs to meet the strict rheological requirements during the printing process, and the nanomaterials should be evenly dispersed to achieve uniformity and precision in printing. (2) The surface properties of the substrate must be sufficiently attractive to the ink when printing different layers of the laminated structure to ensure excellent interface bonding. (3) The moisture absorption and desorption properties of the functional layer and electrode layer need to be precisely designed to match the moisture absorption and desorption deformation of different layers to ensure the long-term working reliability of the device.

This paper develops a fully screen-printable ion diode type moisture-based power generation array. The device has a sandwich stacking structure and can achieve an excellent balance between moisture capture, anion and cation separation, and

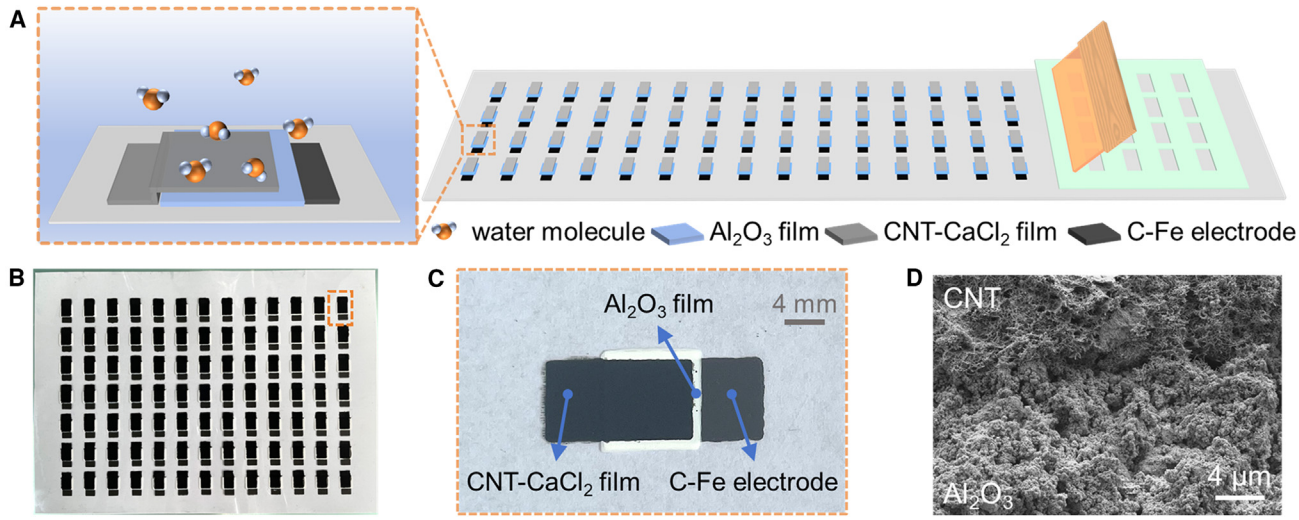

Figure 1. Design and fabrication of moisture-based power generation devices

(A) Schematic diagram of a fully screen-printed moisture-based power generation array.

(B) Optical image of a screen-printed moisture-based power generation array on a flexible PET substrate.

(C) Optical image of a moisture-based power generation unit.

(D) Scanning electron microscope image of the junction between the top electrode and the functional material.

ion-electron charge conversion. The ink parameters of the nano-functional layer and the electrode layer are regulated to make it printable and flexible. The effect of printing process parameters on device performance is studied. In particular, the addition of ethyl cellulose (EC) in the ink simultaneously meets the requirements of rheology, interface bonding, and moisture absorption and desorption deformation matching, improves the mechanical and electrical properties of nano-functional materials, and makes the device reliable. After optimizing the parameters, the device outputs an open circuit voltage of 0.7 V and a short circuit current density of 56.69 $\mu A/cm^2$ at room temperature and 93% RH (relative humidity). Its output power can be further customized after series-parallel integration, demonstrating its wide application prospects for powering small electronic devices. The moisture-based power generation device has the potential for the following practical application scenarios, such as the following: using the device to power sensors in remote areas or in scenarios where it is difficult to replace batteries, or utilizing the humidity difference in human sweat to power small wearable electronic devices, and combining with other renewable energy sources, such as solar energy and wind energy, to supplement the supply of energy with moisture-based power generation to form a hybrid power generation system.

RESULT AND DISCUSSION

Design and manufacture of moisture-based power generation devices

Each power generation unit in the array is a sandwich structure - the upper layer is a CNT-$CaCl_2$ composite electrode, the middle layer is a nano-alumina film, and the lower layer is a C-Fe composite electrode (Figure 1A). The moisture-based power generation unit can be integrated on a large scale by screen printing. In order to achieve complete screen printing of moisture-based power generation devices, it is necessary to formulate printing inks corresponding to each part of the device. The top electrode printing ink is prepared by dispersing carbon nanotubes (CNTs), $CaCl_2$, and EC in a composite solvent of pine alcohol and ethanol. The functional material printing ink is prepared by dispersing nano-alumina particles and EC in pine alcohol and ethanol. EC is introduced into the top electrode and functional material layer to bond CNT or nano-alumina particles and make the functional film flexible. The bottom electrode printing ink is a uniform mixing of micron-sized Fe powder into a commercial conductive C paste. During screen printing, C-Fe composite electrode, nano-alumina film and CNT-$CaCl_2$ electrode are deposited sequentially on a flexible PET substrate using a screen with a custom-designed pattern. Since EC acts as a binder for both CNT and nano-alumina particles, the top electrode and the functional material layer can be tightly bonded. The conductive C paste in the bottom electrode has excellent adhesion and stability, which makes the bottom electrode have a strong bond with the substrate, and the bottom electrode can still maintain a stable structure without being destroyed when printing the functional material and the top electrode.

The moisture-based power generation array with sandwich structure designed in this work has the following advantages. (1) Compared with the planar structure, the contact area between the electrode and the functional material of the sandwich structured device is larger, which is conducive to the collection of charges and the conversion between ion current and electron current. Although the sandwich structure has the disadvantage of a smaller interaction area between moisture and functional materials, the use of CNT-$CaCl_2$ as the top electrode in this work can effectively solve the disadvantage of limited moisture

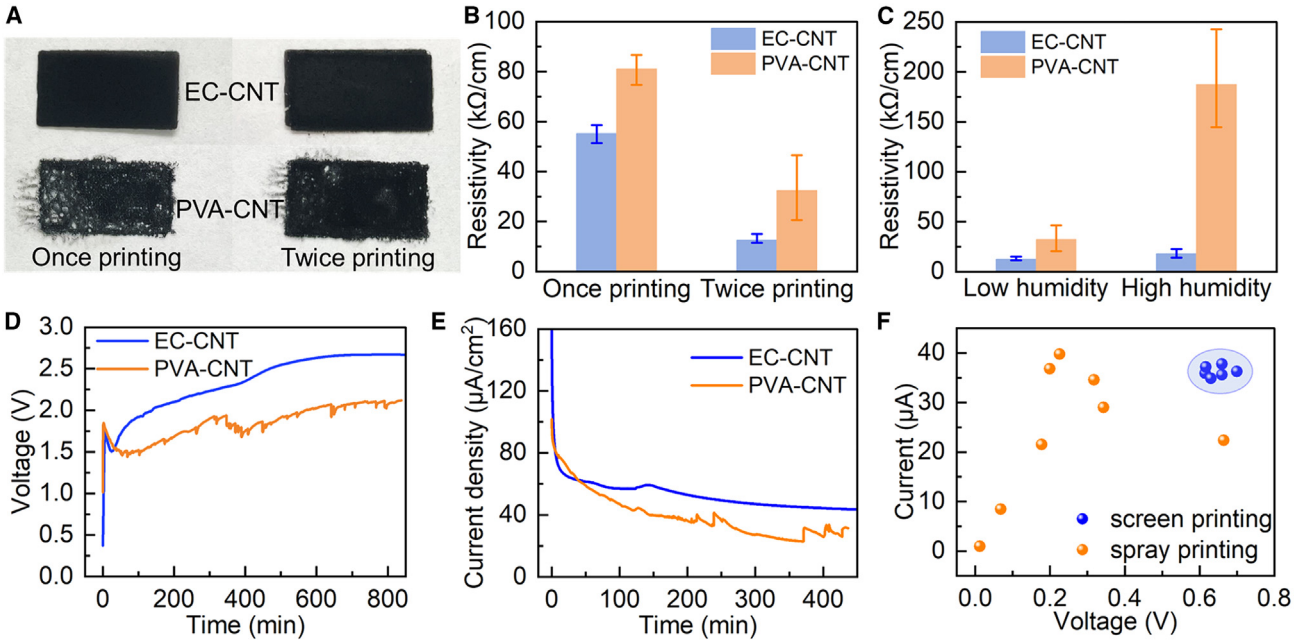

Figure 2. Effect of screen printing parameters on the performance of moisture-based power generation devices

(A) Optical image of top electrodes made by screen printing using ethyl cellulose and PVA as binders.

(B) Resistivity of EC-CNT electrodes and PVA-CNT electrodes.

(C) Resistivity of the two electrodes in low humidity (42% RH) and high humidity (93% RH) environments.

(D and E) Open circuit voltage and short circuit current density test curves of the moisture-based power generation arrays (4 power generation units in series) with top electrodes containing different binders.

(F) Comparison of the power generation performance distribution of moisture-based power generation devices made by screen printing and spraying printing processes.

capture area. Since the CNT film has a porous structure and a large specific surface area, water molecules adsorb and penetrate quickly. In addition, the addition of calcium chloride to the CNT film enhances the hygroscopicity of the top electrode. (2) The three printing inks prepared in this work have good adhesion, so the moisture-based power generation device can be firmly attached to the PET flexible substrate without the need for additional fixing and packaging. (3) Since the moisture-based power generation device in this work is completely manufactured using screen printing, the device has the advantages of simple manufacturing process, low manufacturing cost and large area scalability. As shown in Figure 1B, 13 × 7 moisture-based power generation units have been arrayed on a flexible PET (polyethylene terephthalate) substrate using a screen printing process. A single moisture-based power generation unit photo is shown in Figure 1C, from which it can be seen that the geometric outlines of each part of the screen-printed device are clear and the printing quality is very good. As shown in Figure 1D, the scanning electron microscope image shows that there is an excellent interface connection between the CNT film and the aluminum oxide film.

Effect of screen printing parameters on device performance

To prepare CNT and nano-alumina slurry and form a shape-stable film after printing and drying, it is necessary to select a suitable adhesive and corresponding solvent. Therefore, we investigate the effects of two adhesives, EC and PVA (polyvinyl alcohol), on screen-printed devices. PVA was selected as a control because it is a functional material commonly used in the field of moisture-based power generation. As shown in Figure 2A, EC and PVA were used as adhesives to make top electrode screen-printed slurries, respectively. Screen printing was performed once and twice, and the EC-CNT top electrode and PVA-CNT top electrode were obtained after drying. Regardless of whether it was screen-printed once or twice, the top electrode made with EC as an adhesive had a more regular geometry and higher printing quality, while the control electrode using PVA as an adhesive had blurred edges and uneven CNT distribution. Then, the resistivity of the aforementioned two top electrodes was tested, as shown in Figure 2B. When screen-printed once, the resistivity of the EC-CNT top electrode was 10.3 Ω cm, while the resistivity of the PVA-CNT top electrode was 15.14 Ω cm. When screen-printed twice, the resistivity of the EC-CNT top electrode was 4.7 Ω cm, while the resistivity of the PVA-CNT top electrode was 12.1 Ω cm. The top electrode using EC as a binder has a lower resistivity and better conductivity, which is due to its higher printing quality. In addition, the resistivity of the EC-CNT electrode and PVA-CNT electrode screen-printed twice in low humidity and high humidity environments was also tested, as shown in Figure 2C. In a high humidity environment (93% RH), the resistivity of the EC-CNT top electrode was 6.74 Ω cm, while the resistivity of the

PVA-CNT top electrode was 69.94 Ω cm. In a low humidity environment (42% RH), the resistivity of the EC-CNT top electrode was 4.7 Ω cm, while the resistivity of the PVA-CNT top electrode was 12.1 Ω cm. From the test results, it can be seen that the transition from low humidity to high humidity environment of PVA-CNT electrode makes the resistivity of the electrode increase by more than five times, and the resistivity of PVA-CNT electrode is relatively unstable and fluctuates greatly in high humidity environment, while the resistivity of EC-CNT electrode changes little. This is because in high humidity environment, the top electrode adsorbs a large amount of water molecules, and PVA gradually dissolves in water to produce volume deformation, thereby destroying the structure and morphology of the top electrode, while EC is insoluble in water and relatively stable in high humidity environment.

The aforementioned experimental results illustrate the effect of the adhesive on the top electrode morphology, resistivity, and wet stability. In order to further explore the effect of the two adhesives on the power generation performance, we fabricated a 4 × 1 moisture-based power generation array by screen printing (Figure S1). The top electrode of the experimental group was EC-CNT, and the top electrode of the control group was PVA-CNT. The open circuit voltage and short circuit current density were tested in a high humidity environment (93% RH). The test results are shown in Figures 2D and 2E. It can be seen from the figure that the open circuit voltage and short circuit current density of the EC-CNT experimental group device are higher than those of the PVA-CNT control group, which is due to the relatively lower electrode resistance. In addition, the power generation performance test curve of the control group fluctuates greatly and is unstable, which is due to the random deformation accompanied by dissolution-precipitation during the PVA absorption and dehumidification process. The power generation performance results are consistent with the aforementioned resistivity and wet stability experimental results, which can indirectly explain that the adhesive affects the morphology and resistivity of the top electrode, and then affects the power generation performance of the moisture-based power generation device.

In order to illustrate the advantages of screen printing over other printing processes, moisture-based power generation devices were manufactured by screen printing and spray printing and their performances were tested. The test results are shown in Figure 2F. The performance of the devices manufactured by screen printing is relatively concentrated, while the performance of the devices manufactured by spraying printing is quite discrete. This is because screen printing has more advantages than spray printing in terms of uniformity, which is specifically reflected in printing quality, detail expression, ink control, adaptability, consistency, and simplicity of post-processing.

Analysis of other performance influencing factors

This work uses a simple and low-cost method to create stable humidity environment. Different steady-state humidity environments can be created by adding different types of saturated salt solutions into a closed space. The power generation performance of the moisture-based power generation unit was tested at 25°C and 93% RH, as shown in Figures 3A and S2. A 0.64 cm^2 power generation unit can generate an open circuit voltage of 0.7 V and a short-circuit current density of 56.69 μA/cm^2 Figure 3B shows the output voltage and current density of the moisture-based power generation unit under different external load resistances. Further, the output power density curve of the moisture-based power generation unit under different load resistances can be obtained (Figure S3). When the load resistance is 7 kΩ, the output power density of the moisture-based power generation unit reaches a maximum value of 5.9 μW/cm^2. The effect of different humidity on the power generation performance is shown in Figures 3C and S4. When the relative humidity increases from 15% to 93%, the open circuit voltage and short-circuit current density of the power generation unit increase with the increase in humidity. When the relative humidity is as low as 15%, the power generation unit has almost no power generation performance. At this time, the humidity gradient inside and outside the device is small, which affects the movement and transportation of water molecules and anions and cations.

In addition, we also explore the effects of the thickness of the alumina film and the amount of EC addition on the power generation performance. First, the thickness of the alumina film is controlled by the number of screen printing times. The experimental test results at 25°C and 93% RH are shown in Figures 3D and S5. When the thickness of the alumina film is 56 μm, the open circuit voltage and short circuit current density of the moisture-based power generation unit reach the best, with the open circuit voltage reaching 0.7 V and the short circuit current density reaching 56.69 μA/cm^2. Too small alumina film thickness leads to a decrease in the humidity gradient in the film, which is not conducive to the efficient migration of water molecules and ions. Too large a thickness increases the ion transmission path and increases the internal resistance of the device, which also leads to reduced output performance. Then, the effect of the mass ratio of nano-alumina to EC in the alumina film on the power generation performance was explored. The experimental test results at 25°C and 93%RH are shown in Figures 3E and S6. It can be seen that the optimal mass ratio of nano-alumina to EC is 10:1. As the mass ratio decreases, the power generation performance gradually decreases. Excessive EC will affect the stacking of nano-alumina and the formation of nanopores, thereby reducing the power generation performance. But too little EC will make it difficult to form a stable alumina film. After determining the optimal process parameters of the moisture-based power generation unit, it is compared with some typical moisture-based power generation devices reported in recent years, as shown in Figure 3F and Table S1. It can be seen from the chart that the moisture-based power generation unit in this work has advantages in open circuit voltage, short circuit current density and output power density. More importantly, the power generation unit is completely manufactured by screen printing and has good scalability.

Investigation of power generation principle

In order to explore the relationship between ambient humidity and device power generation, we transferred the device from 93% RH to 0% RH and tested its current output. The results are shown in Figure 4A. When the device was placed in 93% RH, its short-circuit current continued to increase from 0. Then,

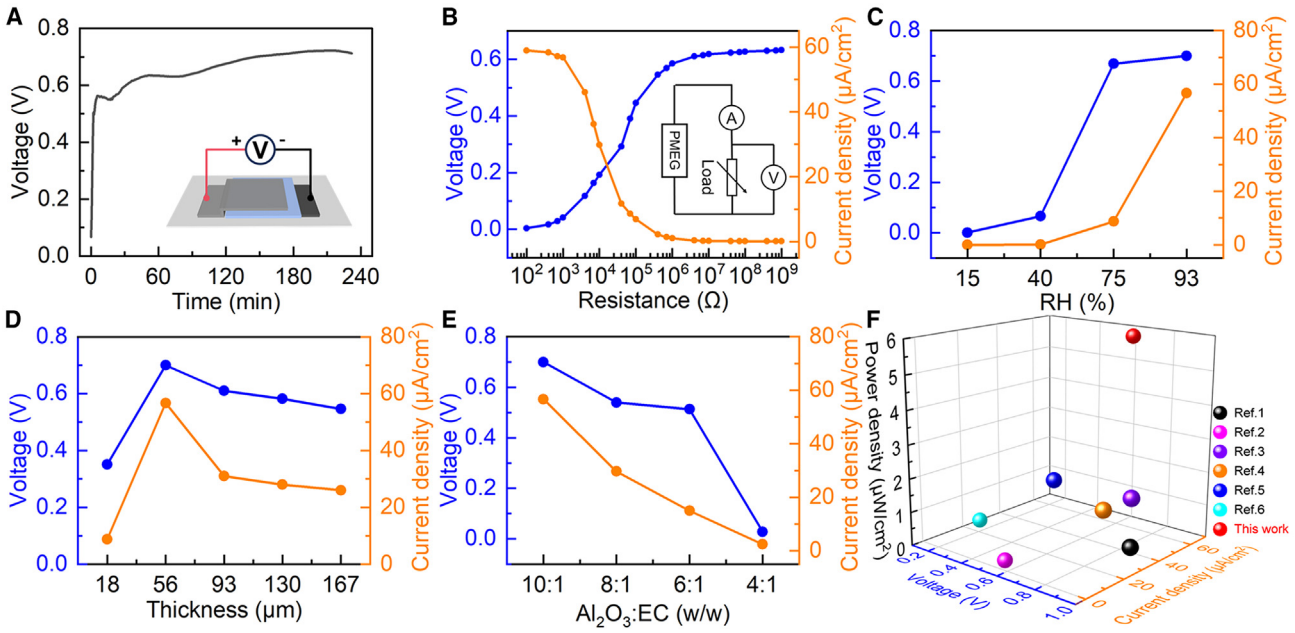

Figure 3. Effect of other factors on moisture-based power generation performance

(A) Open circuit voltage test curve of a small-sized (0.64 cm^2) moisture-based power generation unit (test environment: 25°C, 93% RH, the inset is a schematic diagram of the test wiring).

(B) Open circuit voltage and short circuit current density of the power generation unit under different load conditions (the inset is a load test circuit diagram).

(C) Power generation performance of the power generation unit under different humidity conditions.

(D) Effect of thickness of functional material (alumina film) on power generation performance.

(E) Effect of mass ratio of nano-alumina to ethyl cellulose in functional material on power generation performance.

(F) Comparison of power generation performance of this device with humidity power generation devices in other literature. Note: The references in this figure are in the supplementary materials.

when the device was transferred from 93% RH to 0% RH, its short-circuit current continued to decrease and finally dropped to 0. This shows that moisture is crucial to the power generation of the device. Next, to explore the relationship between nano-alumina, EC and device power generation, we used pure EC as a functional material to manufacture a moisture-based power generation unit and tested its power generation performance under 93% RH conditions. The test results are shown in Figure 4B. It can be seen from the figure that the open circuit voltage and short-circuit current of the device are both 0, indicating that EC is not an important material to generate electrical signals. EC only acts as a binder, which indirectly shows that the power generation of the device is closely related to nano-alumina. Then, in order to explore the relationship between the bottom electrode and the power generation of the device, we used three electrodes (C-Fe, C and Au) as the bottom electrodes of the moisture-based power generation unit and tested its open circuit voltage under 93% RH conditions. The test results are shown in Figure 4C. It can be seen from the figure that the open circuit voltage of the moisture-based power generation unit using inert bottom electrodes (C electrode and Au electrode) can reach 0.15 V under high humidity conditions. This shows that the pure hydrovoltaic effect has a certain contribution to the power generation. After adding active metal (Fe) material to the bottom electrode, the power generation performance can be further improved, and the open circuit voltage reaches 0.7 V.

The top electrode and functional material of the moisture-based power generation unit were characterized by microscopic morphology. Figure 4D shows a scanning electron microscope image of the top electrode (EC-CNT), and Figure 4E shows a scanning electron microscope image of the functional material aluminum oxide film. It can be seen from the figure that both the top electrode and the functional material layer have a large number of micro-nanopores, which are conducive to the adsorption and penetration of moisture and the transport of ions. Then, the zeta potential of CNT and nano-alumina was tested. As shown in Figure 4F, the zeta potential of CNT is −26.1 mV, and the zeta potential of nano-alumina is 31.1 mV. That is, a PN junction selective for ion transport is easily formed between CNT and nano-alumina. The rectification curve of the moisture-based power generation unit was tested under high humidity and ambient humidity conditions. As shown in Figures 4G and S7, a bias voltage of ±1 V was applied to the device and its I-V curve was tested. It can be seen from the figure that under high humidity or ambient humidity conditions, the moisture-based power generation unit has a strong ion diode rectification effect. This is because after the CNT-nano-alumina combination, the contact interface generates a built-in electric field pointing from the alumina to the top electrode. When a forward bias voltage is applied, the direction of the external electric field is opposite to the direction of the device's built-in electric field, thereby weakening the electric field, resulting in weaker anion and cation

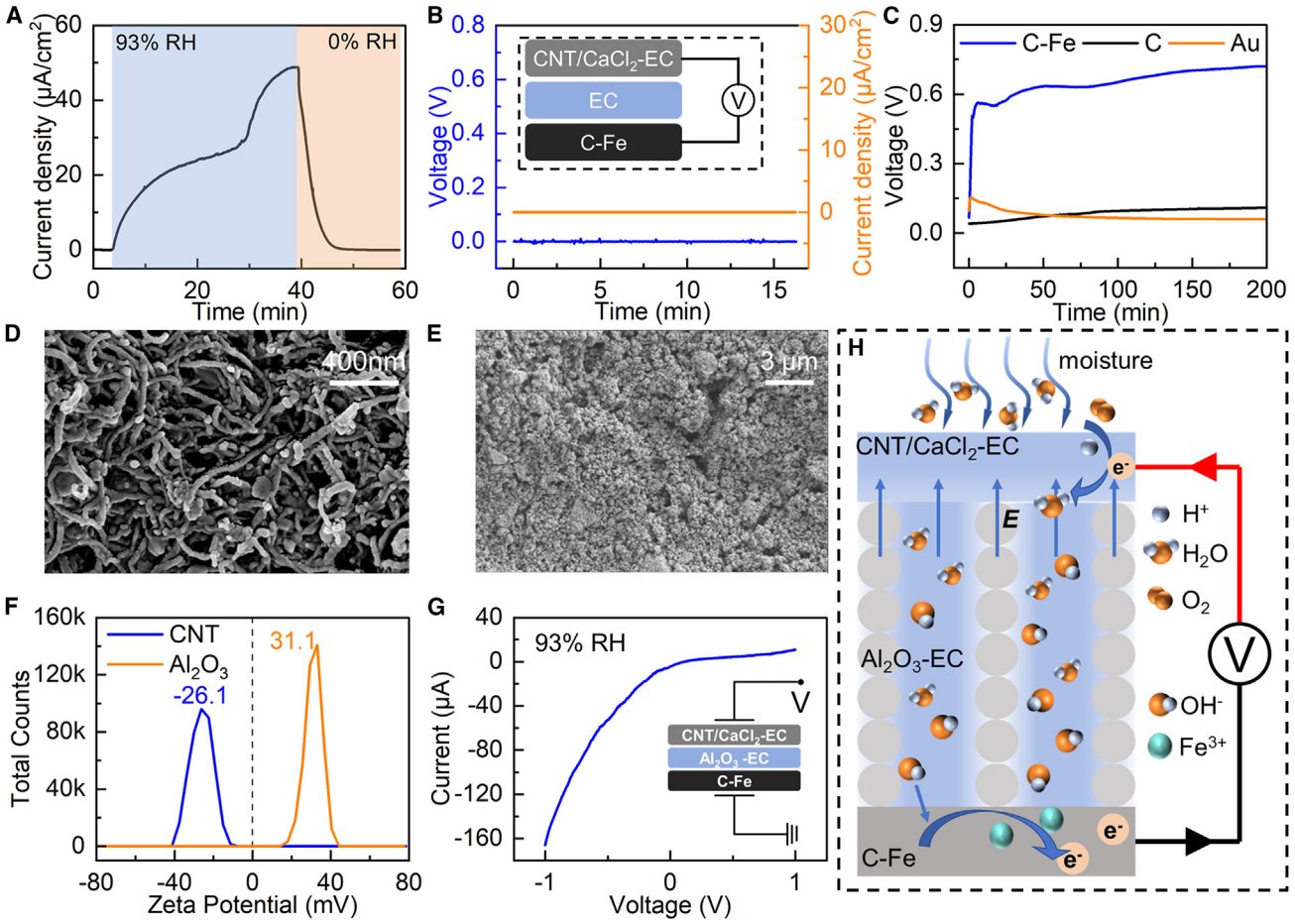

Figure 4. Exploration of the power generation principle

(A) Current output of the moisture-based power generation unit under 93% RH and 0% RH conditions.
(B) Power generation performance of the device when ethyl cellulose is used as the functional material.
(C) Open circuit voltage of the moisture-based power generation unit with different bottom electrodes.
(D) Scanning electron microscope image of the EC-CNT top electrode.
(E) Scanning electron microscope image of the alumina film.
(F) Zeta potential of CNT and nano-alumina.
(G) Rectification curve of the power generation unit under high humidity environment.
(H) Schematic diagram of the power generation principle of the moisture-based power generation unit.

separation, which reduces device performance. When a reverse bias voltage is applied, the direction of the external electric field is the same as the direction of the device's built-in electric field, which promotes the directional movement of anions and cations in the opposite direction, thereby significantly improving the performance of the device.

In summary, the power generation process of the moisture-based power generation unit is a process of the combined action of the hydrovoltaic effect, the ion diode rectification effect, and the redox reaction. Figure 4H shows the power generation principle of the moisture-based power generation unit. The top electrode CNT/$CaCl_2$ film adsorbs water molecules in the air and dissociates into freely moving hydrogen ions and hydroxide ions (as well as chloride ions and calcium ions). Under the combined action of the humidity gradient and the built-in electric field, the negatively charged anions move from the top electrode to the bottom electrode through the nanochannel, realizing the separation of anions and cations. In addition, the reduction reaction involving hydrogen ions and the oxidation reaction involving hydroxide ions occur near the top electrode and the bottom electrode, respectively, so that the ion current is converted into an electron current, thereby realizing the output of electrical energy.

Integration and application of moisture-based power generation units

The moisture-based power generation unit is manufactured by full screen printing process, which is very easy to achieve large-area integration. Figure S8 shows the method of large-area integration of moisture-based power generation units. The open circuit voltage of the power generation array can be effectively regulated by the series integration method, and the short-circuit current of the array can be regulated by the parallel integration

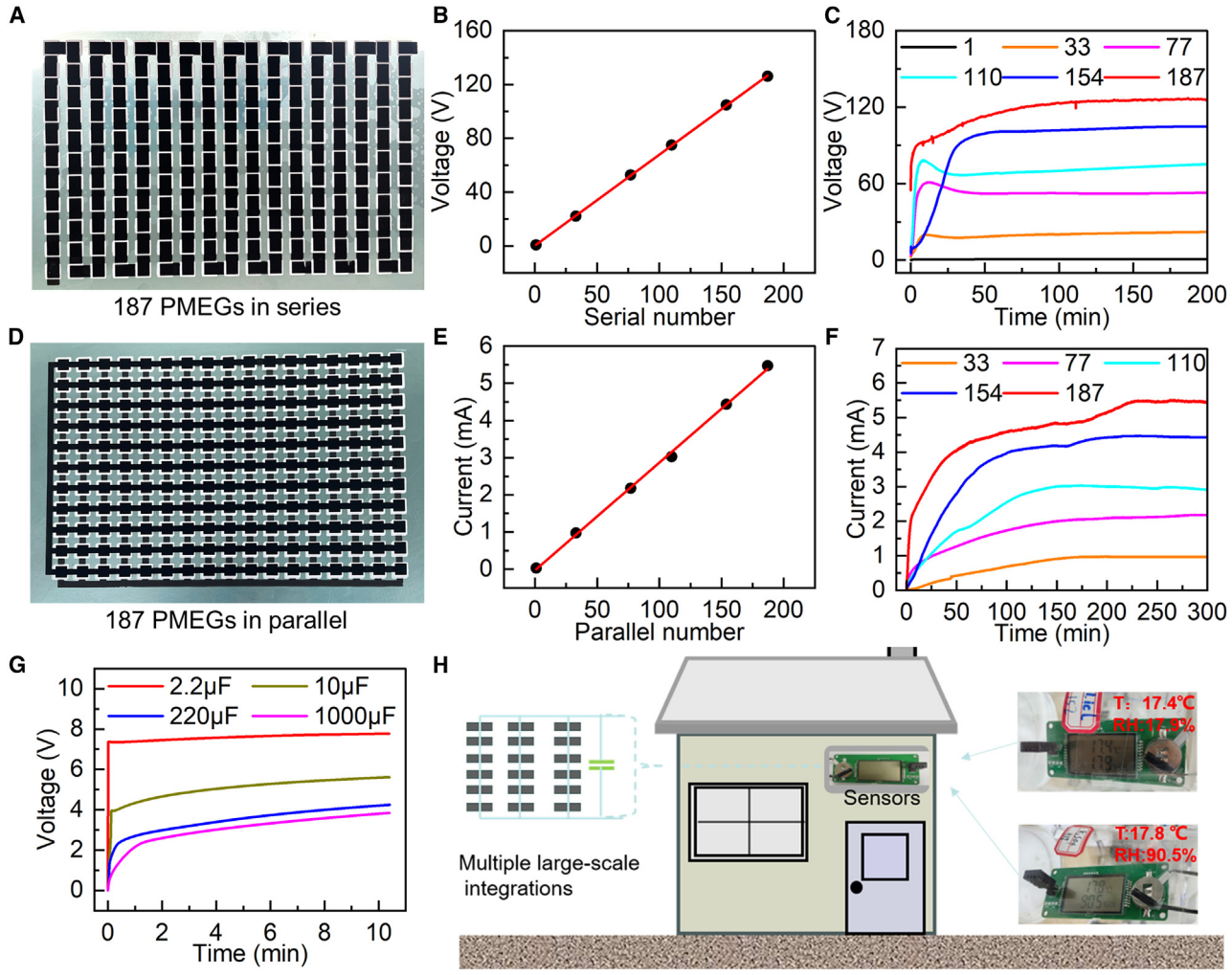

Figure 5. Large-area integration and application of moisture-based power generation units

(A) Optical image of an array of 187 power generation units in series.

(B and C) Open circuit voltage of different numbers of power generation units in series.

(D) Optical image of an array of 187 power generation units in parallel.

(E and F) Short circuit current of different numbers of power generation units in parallel.

(G) Using a moisture-based power generation array to charge different capacitors.

(H) A power supply combining arrays of devices and capacitors can power a temperature and humidity sensing system to detect temperature and humidity data in outdoor environments.

method. Series integration is achieved by partially overlapping the top electrode of each power generation unit with the bottom electrode of the next unit, while parallel integration is a vertical cross arrangement of the interdigitated top electrode and the interdigitated bottom electrode, and the functional material of nano-aluminum film is located at the intersection and isolates the upper and lower electrodes to prevent short circuit. Figure 5A shows an array of 187 power generation units in series manufactured by screen printing on the surface of an A4-sized flexible PET film. Figures 5B and 5C show that the open circuit voltage of the power generation array increases linearly with the increase in the number of units in series. The open circuit voltage of a single moisture-based power generation unit is 0.7 V, and an array of 187 power generation units in series can generate an open circuit voltage of 126 V Figure 5D shows an array of 187 power generation units in parallel fabricated by screen printing on the surface of an A4-sized flexible PET film. Figures 5E and 5F illustrate that the short-circuit current of the power generation array increases linearly with the increase in the number of power generation units in parallel. The short-circuit current of a single power generation unit is 36 μA, and an array of 187 power generation units in parallel can generate a short-circuit current of 5.47 mA. After achieving large-area integration of moisture-based power generation units, we demonstrated a series of applications. We used the power generation array to charge different commercial capacitors, as shown in Figure 5G. A 2.2 μF capacitor can be charged instantly, and a 1,000 μF capacitor can be charged to 3 V within 10 min. In addition, as shown in Figure 5H,

we use seven large-area array devices in combination with capacitors as a power source to power the temperature and humidity monitoring system (on the right side, the system detecting different humidity environments). In this way, the temperature and humidity changes in places such as houses, computer rooms, vegetable greenhouses, etc. can be displayed in real time.

Conclusion

In this work, we developed a large-area printable moisture-based power generation array device based on a sandwich structure through screen printing. The sandwich structure helps the device achieve an excellent balance between moisture capture, anion and cation separation, and ion-electron charge conversion. The ink regulation and manufacturing strategy compatible with the screen printing process enables the power generation array device to have uniform, high-performance, reliable electrical output and high cost-effectiveness. Our power generation device can achieve customized power output through a series-parallel integration strategy. For example: in a high humidity (93% RH) environment, the open-circuit voltage generated by an A4-sized series-parallel integrated array can reach 126 V, and the short-circuit current generated can reach 5.47 mA. The integrated flexible array can drive many commercial electronic devices, such as calculators, LED (light emitting diode) lights, etc., demonstrating its broad application prospects for powering small electronic devices. Overall, the moisture-based power generation device shows high performance for the following reasons: (1) the ion diode structure facilitates the fast movement of ions, (2) the sandwich stack structure has a larger PN junction area and a larger electrode charge collection area relative to the planar device structure, (3) the coupling of the redox reaction with the ion rectification effect further improves the power generation performance of the device, and (4) the device can be manufactured using screen printing, so its properties can be customized.

Limitations of the study

Current research still uses active metal electrodes, which inevitably introduces energy from chemical reactions, not pure green energy. In addition, active electrodes will also be passivated, causing the performance of the device to deteriorate after long-term operation. Future research should explore hydrovoltaic power generation devices and manufacturing technologies that are not coupled with active electrodes.

RESOURCE AVAILABILITY

Lead contact

Further information and requests for resources should be directed to and will be fulfilled by the lead contact, Dr. Tingting Yang (yangtingting@swjtu.edu.cn).

Materials availability

This study did not generate new unique reagents. All chemicals were obtained from commercial resources and used as received.

Data and code availability

- Data reported in this paper will be shared by the lead contact upon reasonable request.
- This study does not report any original code.
- Any additional information required to reanalyze the data reported in this paper is available from the lead contact upon reasonable request.

ACKNOWLEDGMENTS

The authors acknowledge the financial support from the Chengdu University Talent Introduction Project (project no: X2060), Natural Science Foundation of Sichuan Province (nos. 2023NSFSC0981 and 2023NSFSC1988), Fundamental Research Funds for the Central Universities in China (grant nos. SWJTU 2682024CG012, 2682023QZ004, 2682023ZTPY001, 2682023KJ012, and 268 2022KJ017).

AUTHOR CONTRIBUTIONS

T.Y. and J.Z. designed the research. T.Y. directed this research. J.Z. wrote the paper. J.Z. and Y.Y. conducted the majority of the experimental work. X.Z. proposed mechanisms.

DECLARATION OF INTERESTS

The authors declare no competing interests.

STAR★METHODS

Detailed methods are provided in the online version of this paper and include the following:

- KEY RESOURCES TABLE
- METHOD DETAILS
  - Synthesis of top electrode ink
  - Synthesis of functional material ink
  - Synthesis of bottom electrode ink
  - Screen printing preparation process
  - Electrical output measurement
  - Material characterization
- QUANTIFICATION AND STATISTICAL ANALYSIS

SUPPLEMENTAL INFORMATION

Supplemental information can be found online at https://doi.org/10.1016/j.isci.2025.112026.

Received: August 18, 2024
Revised: December 11, 2024
Accepted: February 11, 2025
Published: February 15, 2025

REFERENCES

1. Zhang, Z., Li, X., Yin, J., Xu, Y., Fei, W., Xue, M., Wang, Q., Zhou, J., and Guo, W. (2018). Emerging hydrovoltaic technology. Nat. Nanotechnol. *13*, 1109–1119. https://doi.org/10.1038/s41565-018-0228-6.
2. Shen, D., Duley, W.W., Peng, P., Xiao, M., Feng, J., Liu, L., Zou, G., and Zhou, Y.N. (2020). Moisture-enabled electricity generation: from physics and materials to self-powered applications. Adv. Mater. *32*, 2003722. https://doi.org/10.1002/adma.202003722.
3. Chen, Z., Shi, J., Li, Y., Ma, B., Yan, X., Liu, M., Jin, H., Li, D., Jing, D., and Guo, L. (2021). Recent progress of energy harvesting and conversion coupled with atmospheric water gathering. Energy Convers. Manag. *246*, 114668. https://doi.org/10.1016/j.enconman.2021.114668.
4. Huang, Y., Cheng, H., and Qu, L. (2021). Emerging materials for water-enabled electricity generation. ACS Mater. Lett. *3*, 193–209. https://doi.org/10.1021/acsmaterialslett.0c00474.
5. Wang, K., and Li, J. (2021). Electricity generation from the interaction of liquid-solid interface: a review. J. Mater. Chem. A Mater. *9*, 8870–8895. https://doi.org/10.1039/d0ta12073a.

6. Sun, Z., Wen, X., Wang, L., Ji, D., Qin, X., Yu, J., and Ramakrishna, S. (2022). Emerging design principles, materials, and applications for moisture-enabled electric generation. eScience *2*, 32–46. https://doi.org/10.1016/j.esci.2021.12.009.

7. Yan, H., Liu, Z., and Qi, R. (2022). A review of humidity gradient-based power generator: devices, materials and mechanisms. Nano Energy *101*, 107591. https://doi.org/10.1016/j.nanoen.2022.107591.

8. Xu, T., Ding, X., Cheng, H., Han, G., and Qu, L. (2024). Moisture-enabled electricity from hygroscopic materials: a new type of clean energy. Adv. Mater. *36*, 2209661. https://doi.org/10.1002/adma.202209661.

9. Li, M., Zong, L., Yang, W., Li, X., You, J., Wu, X., Li, Z., and Li, C. (2019). Biological nanofibrous generator for electricity harvest from moist air flow. Adv. Funct. Mater. *29*, 1901798. https://doi.org/10.1002/adfm.201901798.

10. Wang, H., Cheng, H., Huang, Y., Yang, C., Wang, D., Li, C., and Qu, L. (2020). Transparent, self-healing, arbitrary tailorable moist-electric film generator. Nano Energy *67*, 104238. https://doi.org/10.1016/j.nanoen.2019.104238.

11. Chen, S., Xia, H., and Ni, Q.Q. (2021). A wearable sustainable moisture-induced electricity generator based on rGO/GO/rGO sandwich-like structural film. Adv. Electron. Mater. *7*, 2100222. https://doi.org/10.1002/aelm.202100222.

12. Li, Y., Cui, J., Shen, H., Liu, C., Wu, P., Qian, Z., Duan, Y., and Liu, D. (2022). Useful spontaneous hygroelectricity from ambient air by ionic wood. Nano Energy *96*, 107065. https://doi.org/10.1016/j.nanoen.2022.107065.

13. Sun, Z., Wen, X., Wang, L., Yu, J., and Qin, X. (2022). Capacitor-inspired high-performance and durable moist-electric generator. Energy Environ. Sci. *15*, 4584–4591. https://doi.org/10.1039/d2ee02046g.

14. Wang, H., He, T., Hao, X., Huang, Y., Yao, H., Liu, F., Cheng, H., and Qu, L. (2022). Moisture adsorption-desorption full cycle power generation. Nat. Commun. *13*, 2524. https://doi.org/10.1038/s41467-022-30156-3.

15. Zhang, J., Hou, Y., Lei, L., and Hu, S. (2022). Moist-electric generators based on electrospun cellulose acetate nanofiber membranes with tree-like structure. J. Membr. Sci. *662*, 120962. https://doi.org/10.1016/j.memsci.2022.120962.

16. Zhang, R., Qu, M., Wang, H., Fan, M., Chen, Q., Tang, P., and Bin, Y. (2022). Moist-electric films based on asymmetric distribution of sodium alginate oxygen-containing functional groups. React. Funct. Polym. *181*, 105421. https://doi.org/10.1016/j.reactfunctpolym.2022.105421.

17. Zhao, Q., Jiang, Y., Duan, Z., Yuan, Z., Zha, J., Wu, Z., Huang, Q., Zhou, Z., Li, H., He, F., et al. (2022). A Nb_2CT_x/sodium alginate-based composite film with neuron-like network for self-powered humidity sensing. Chem. Eng. J. *438*, 135588. https://doi.org/10.1016/j.cej.2022.135588.

18. Wen, X., Sun, Z., Xie, X., Zhou, Q., Liu, H., Wang, L., Qin, X., and Tan, S.C. (2023). High-performance fully stretchable moist-electric generator. Adv. Funct. Mater. *34*, 2311128. https://doi.org/10.1002/adfm.202311128.

19. Xu, C., Fu, C., Jiang, Z., Yang, T., and Xin, M. (2023). Hygroelectric generator based on antisymmetric modification of graphene spheres with ionic hydrogels. ACS Appl. Nano Mater. *6*, 5930–5938. https://doi.org/10.1021/acsanm.3c00314.

20. Wang, H., Sun, Y., He, T., Huang, Y., Cheng, H., Li, C., Xie, D., Yang, P., Zhang, Y., and Qu, L. (2021). Bilayer of polyelectrolyte films for spontaneous power generation in air up to an integrated 1,000 V output. Nat. Nanotechnol. *16*, 811–819. https://doi.org/10.1038/s41565-021-00903-6.

21. Feng, Z., Zhao, W., Yang, Z., Deng, Y., Yang, T., and Ni, Y. (2022). Energy harvesting by vitrimer-based moist-electric generators. J. Mater. Chem. A Mater. *10*, 11524–11534. https://doi.org/10.1039/d1ta11029b.

22. Yang, S., Tao, X., Chen, W., Mao, J., Luo, H., Lin, S., Zhang, L., and Hao, J. (2022). Ionic hydrogel for efficient and scalable moisture-electric generation. Adv. Mater. *34*, 2200693. https://doi.org/10.1002/adma.202200693.

23. He, T., Wang, H., Lu, B., Guang, T., Yang, C., Huang, Y., Cheng, H., and Qu, L. (2023). Fully printed planar moisture-enabled electric generator arrays for scalable function integration. Joule *7*, 935–951. https://doi.org/10.1016/j.joule.2023.04.007.

24. Huang, Y., Zhou, K., Cheng, H., He, T., Wang, H., Bai, J., Yang, C., Guang, T., Yao, H., Li, F., et al. (2023). Three-dimensional printing of high-performance moisture power generators. Adv. Funct. Mater. *34*, 2308620. https://doi.org/10.1002/adfm.202308620.

25. Li, Q., Qin, Y., Cheng, D., Cheng, M., Zhao, H., Li, L., Qu, S., Tan, J., and Ding, J. (2023). Moist-electric generator with efficient output and scalable integration based on carbonized polymer dot and liquid metal active electrode. Adv. Funct. Mater. *33*, 2211013. https://doi.org/10.1002/adfm.202211013.

26. Yao, Y., Lu, X., Fu, C., Zhang, Y., Fang, J., Qin, J., He, Q.C., and Yang, T. (2023). Patterned coating of ionic diode arrays toward flexible moist-electric generators to power wireless sensor nodes. Adv. Funct. Mater. *34*, 2311465. https://doi.org/10.1002/adfm.202311465.

27. Lu, X., Yang, T., Fu, C., Jiang, Z., Zhang, Y., Shang, K., He, C., Zhou, J., and He, Q.C. (2022). Hierarchically porous fiber-based nanofluidic diode as an efficient multimode hygroelectric generator. Adv. Energy Mater. *12*, 2202634. https://doi.org/10.1002/aenm.202202634.

28. Zhang, Y., Yang, T., Shang, K., Guo, F., Shang, Y., Chang, S., Cui, L., Lu, X., Jiang, Z., Zhou, J., et al. (2022). Sustainable power generation for at least one month from ambient humidity using unique nanofluidic diode. Nat. Commun. *13*, 3484. https://doi.org/10.1038/s41467-022-31067-z.

29. Fang, J., Zhang, X., Duan, P., Jiang, Z., Lu, X., Fu, C., Zhang, Y., Yao, Y., Shang, K., Qin, J., et al. (2024). Efficient and cold-tolerant moisture-enabled power generator combining ionic diode and ionic hydrogel. Mater. Horiz. *11*, 1261–1271. https://doi.org/10.1039/d3mh01496g.

30. Fu, C., Zhou, J., Lu, X., Feng, H., Zhang, Y., Shang, K., Jiang, Z., Yao, Y., He, Q.C., and Yang, T. (2024). A long life moisture-enabled electric generator based on ionic diode rectification and electrode chemistry regulation. Adv. Sci. *11*, 2305530. https://doi.org/10.1002/advs.202305530.

STAR★METHODS

KEY RESOURCES TABLE

REAGENT or RESOURCE	SOURCE	IDENTIFIER
Chemicals, peptides, and recombinant proteins		
Multi-walled Carbon Nanotubes (MWCNTs)	Timesnano Co., Ltd	9004-57-3
Ethyl cellulose M70 (EC)	Sinopharm Chemical Reagent Co., Ltd	10043-52-4
calcium chloride ($CaCl_2$, AR)	Sinopharm Chemical Reagent Co., Ltd	64-17-5
ethanol	Sinopharm Chemical Reagent Co., Ltd	344-28-1
Al_2O_3	Xfnano Co., Ltd	7439-89-6
Iron powder	Shanghai Aladdin Biochemical Technology Co., Ltd	8000-41-7
Terpineol	Macklin Biochemical Technology Co., Ltd	9004-57-3
Multi-walled Carbon Nanotubes (MWCNTs)	Timesnano Co., Ltd	9004-57-3
Ethyl cellulose M70 (EC)	Sinopharm Chemical Reagent Co., Ltd	10043-52-4

METHOD DETAILS

Synthesis of top electrode ink

First, add 3 mL of anhydrous ethanol and 5 mL of pine alcohol to a 30 mL sealable glass bottle, then add 177.57 mg of calcium chloride, and completely dissolve the calcium chloride by magnetic stirring. Then, add 0.3 g of EC to the above solution, and stir it in a water bath until it is completely dissolved at 80° C with 400 r/min. Finally, add 350 mg of CNT to the above solution and stir evenly. The printable top electrode ink is prepared by the above process.

Synthesis of functional material ink

First, add 1 mL of anhydrous ethanol and 8 mL of pine alcohol to a 30 mL sealed glass bottle, then add 0.3 g of EC, place it in a water bath and stir until it is completely dissolved, the temperature is 80°C, and the speed is 400 r/min. Finally, add 3 g of nano-alumina to the above solution and stir evenly. The printable functional material ink is prepared through the above process.

Synthesis of bottom electrode ink

Conductive carbon paste and iron powder are uniformly mixed in a mass ratio of 1:1 by electric stirring to prepare printable bottom electrode ink.

Screen printing preparation process

First, the bottom electrode ink is screen printed and dried on a hot plate at 80°C to obtain the bottom electrode. In addition, the functional material layer and the top electrode are manufactured separately by the same method. The screen used in the above process is 100 mesh.

Electrical output measurement

The device output V_{OC} and I_{SC} were recorded by an electrometer (Keithley 6514), digit multimeter (Keithley DMM7510), and SourceMeter (Keithley 2450). The I-V rectification curves of devices were tested by linear scanning voltammetry using CHI electrochemical analyzer (CHI760E, CH Instruments, Inc, US).

Material characterization

Scanning electron microscope (SEM) (Sigma 300) was used to characterize the morphology of Al_2O_3-EC film and CNT-$CaCl_2$ film. The surface zeta potential of Al_2O_3 and MWCNTs in a neutral environment was measured using a Zeta potential tester (Anton Paar beyond 3, Australia).

QUANTIFICATION AND STATISTICAL ANALYSIS

There is no statistical analysis or quantification in this paper. Figures are produced in Origin from the raw data.